photonics

MDPI

Article

Finite Temperature Ultraviolet-Visible Dielectric Functions of Tantalum Pentoxide: A Combined Spectroscopic Ellipsometry and First-Principles Study

Wenjie Zhang [1,2,†], Zhaohui Zeng [3,†], Tao Cheng [1], Tianhao Fei [1], Zhiwei Fu [4], Xiaoyan Liu [5], Jingyi Zhang [6] and Jia-Yue Yang [1,2,*]

1 School of Energy and Power Engineering, Shandong University, Jinan 250061, China; zhangwenjie@sdu.edu.cn (W.Z.); tao_c@mail.sdu.edu.cn (T.C.); fth@mail.sdu.edu.cn (T.F.)
2 Optics & Thermal Radiation Research Center, Institute of Frontier and Interdisciplinary, Shandong University, Qingdao 266237, China
3 Institute of Semiconductors, Guangdong Academy of Sciences, Guangzhou 510650, China; zengzhaohui@gdisit.com
4 Science and Technology on Reliability Physics and Application of Electronic Component Laboratory, The 5th Electronics Research Institute of the Ministry of Industry and Information Technology, Guangzhou 511370, China; fzw19940124@163.com
5 Institute for Advanced Interdisciplinary Research (IAIR), University of Jinan, Jinan 250022, China; ifc_liuxy@ujn.edu.cn
6 Science and Technology on Advanced Functional Composites Laboratory, Aerospace Research Institute of Materials and Processing Technology, Beijing 100076, China; zhangjingyi712@163.com
* Correspondence: jy_yang@sdu.edu.cn
† These authors contribute equally to this work.

Abstract: Tantalum pentoxide (Ta_2O_5) has demonstrated promising applications in gate dielectrics and microwave communication devices with its intrinsically high dielectric constant and low dielectric loss. Although there are numerous studies on the dielectric properties of Ta_2O_5, few studies have focused on the influence of external environmental changes (i.e., temperature and pressure) on the dielectric properties and the underlying physics is not fully understood. Herein, we synthesize Ta_2O_5 thin films using the magnetron sputtering method, measure the ultraviolet-visible dielectric function at temperatures varying from 300 to 873 K by spectroscopic ellipsometry (SE), and investigate the temperature influence on the dielectric function from first principles. SE experiments observe that temperature has a nontrivial influence on the ultraviolet-visible dielectric function, accompanying the consistently decreased amplitude and increased broadening width for the dominant absorption peak. First-principles calculations confirm that the dominant absorption peak originates from the aggregated energy states near the valence band maximum (VBM) and conduction band minimum (CBM), and the theoretically predicted dielectric functions demonstrate good agreement with the SE experiments. Moreover, by performing first-principles molecular dynamics simulations, the finite-temperature dielectric function is predicted and its change trend with increasing temperature agrees overall with the SE measurements. This work explores the physical origins of temperature influence on the ultraviolet-visible dielectric function of Ta_2O_5, aimed at promoting its applications in the field of micro-/nanoelectronics.

Keywords: dielectric function; spectroscopic ellipsometry; first-principles; temperature dependence

Citation: Zhang, W.; Zeng, Z.; Cheng, T.; Fei, T.; Fu, Z.; Liu, X.; Zhang, J.; Yang, J.-Y. Finite Temperature Ultraviolet-Visible Dielectric Functions of Tantalum Pentoxide: A Combined Spectroscopic Ellipsometry and First-Principles Study. *Photonics* **2022**, *9*, 440. https://doi.org/10.3390/photonics9070440

Received: 16 May 2022
Accepted: 20 June 2022
Published: 22 June 2022

1. Introduction

High-performance dielectric materials have been attracting great attention as they show great advantages in various miniaturized devices and high-density storage applications [1,2]. High dielectric constant oxides have become a key carrier for current microelectronic applications such as dynamic random access memory (DRAM) devices and on-chip

capacitors [3]. Tantalum pentoxide (Ta_2O_5) stands out among binary metal oxides due to its intrinsically high dielectric constant, low dielectric loss, high chemical and thermal stability, and high compatibility with current silicon-based microelectronic devices [4,5]. In addition, Ta_2O_5 has received considerable attention for its promising applications in resistive random access memory (RRAM) devices [6,7], gate dielectrics [8] and high-average-power lasers [9], as well as dielectric resonators in microwave communication devices [10]. To promote such a large variety of applications, a deep understanding of the dielectric function of Ta_2O_5 is of great necessity.

The dielectric function, $\varepsilon = \varepsilon_1 + i\varepsilon_2$, is one of the fundamental thermophysical quantities which reflects the intrinsic light–matter interactions in solids [11]. Numerous studies have focused on understanding dielectric characteristics of Ta_2O_5 [12–15] either using spectroscopic ellipsometry (SE) experiments or performing first-principles simulations. SE is a nondestructive optical technique which is based on measuring the change in the polarization state of incident light to precisely determine optical constants, without the use of Kramers–Kronig (KK) analysis [16–21]. With the aid of SE, several studies have obtained valuable information regarding the structural [22,23] and optical [24–26] characteristics of Ta_2O_5. Darmasetiawan and co-workers performed ellipsometric measurements on Ta_2O_5 thin films deposited on Si(100) substrates and obtained the refractive index with high accuracy [27]. To gain a deeper understanding of dielectric properties, atomistic scale first-principles simulations have been performed. The first-principles method is an effective tool to study electrons' quantum behaviors and to predict physical properties of condensed matter with high accuracy [28–31]. J. Lee et al. [30] further investigated the thermodynamic, electronic, and optical properties of oxygen vacancies in amorphous Ta_2O_5 based on the hybrid generalized density functional theory, and the calculation results were consistent with experimental measurements. C. Valencia-Balvin et al. [32] presented a theoretical study on electronic and dielectric properties of λ-Ta_2O_5 using the density generalized function theory and the results obtained were in agreement with the literature values. M. V. Ivanov et al. [29] studied the electronic structure of δ-Ta_2O_5 with oxygen vacancy and found that the oxygen vacancy induced a defect state in the energy gap 1.2 eV above the top of the valence band. Moreover, the thermal stabilities of optical components have been shown to strongly influence the performance of optical wave systems [33]. For example, high temperature-induced spectral drift can pose a challenge in the design of laser channels. Liu et al., based on the conventional solid-state reaction method and advanced irradiation technique, investigated the high temperature phase and showed that high temperature greatly changed the lattice structures [34]. However, few studies have focused on the influence of external environmental conditions, as represented by temperature, on the dielectric properties of Ta_2O_5. Although Chu et al. [33] investigated the effect of temperature on the refractive index of Ta_2O_5, the upper temperature limit studied was too low to effectively characterize the effect of high temperature. Therefore, experimental data on the high-temperature dielectric function of Ta_2O_5 are urgently needed. Furthermore, the first-principles calculations will facilitate further insight into the mechanism of temperature variation of the dielectric function. These works are expected to provide theoretical guidance for the practical applications of Ta_2O_5-based optoelectronic materials.

In this work, we apply the magnetron sputtering method to synthesize Ta_2O_5 thin films, and combine SE measurements and first-principles simulations to systematically study the ultraviolet-visible dielectric function and its temperature dependence. SE experiments show that the dominant dielectric absorption peak of Ta_2O_5 changes consistently as temperature increases, accompanied by decreased amplitude and broadened width, which can be intrinsically interpreted by analyzing the electronic band structure and density of states from first-principles calculations.

2. Materials and Methods

The Ta_2O_5 thin films were prepared using the magnetron sputtering method. Firstly, a 2-inch quartz glass with the thickness of 500 nm was chosen as the substrate and was

cleaned with an ultrasonic washer for 15 min (5 min with acetone, 5 min with isopropanol, and 5 min with ethanol absolute). The Ta_2O_5 thin films were coated with the Kurt J. Lesker PVD 75 using the RF power of 100 W. During the deposition, the sputtering atmosphere was mixed with 10% oxygen and 90% nitrogen gas. The growth temperature was set as 300 K, working pressure was 3 m Torr and the deposition duration was 7200 s. After the Ta_2O_5 thin films were prepared, we performed an X-ray diffraction (XRD) analysis and observed a continuous diffraction pattern, suggesting the noncrystalline phase.

To obtain the ultraviolet-visible dielectric function and thickness of the Ta_2O_5 thin films, we employed the RC2 ellipsometer purchased from J.A. Woollam Company. After measuring the basic ellipsometric parameters (Ψ, Δ), an optical oscillator model was built to extract the film thickness and dielectric function. The film thickness was determined as 245 nm, consistent with the measured 230 nm by Profilometer. Moreover, to measure the dielectric function at varying temperatures, we employed a Linkham heat cell to heat samples up to 873 K and pure dry nitrogen gas was continuously injected into the sample container to remove oxygen and to prevent oxidation of the samples. When the temperature fluctuation was less than 0.1 K, the ellipsometric data were measured and the temperature-dependent dielectric function was obtained. The measured spectral range was 196–1690 nm and the spectral resolution was set as 1 nm. With the use of a heat cell, the incident angle was fixed as 70°.

In semiconductors, the dielectric function originates from the electronic interband transitions. Following Fermi's golden rule, the imaginary part of dielectric function ε_2 can be evaluated by [35]:

$$\begin{aligned}\varepsilon^2_{\alpha\beta} = \left(\tfrac{2e\hbar^2}{m\omega}\right)^2 \tfrac{1}{\Omega} \lim_{\mathbf{q}\to 0} \sum_{c,v,\mathbf{k}} 2w_{\mathbf{k}}\delta(E_c - E_v - \hbar\omega) \\ \times \langle \varphi_{c\mathbf{k}} | i\nabla_\alpha - \mathbf{k}_\alpha | \varphi_{v\mathbf{k}} \rangle \langle \varphi_{c\mathbf{k}} | i\nabla_\beta - \mathbf{k}_\beta | \varphi_{v\mathbf{k}} \rangle^*,\end{aligned} \tag{1}$$

where Ω is the volume of unit cell; $\hbar$ is the reduced Planck's constant; e and m are the electron charge and mass, respectively; φ is the electronic wave function; w_k is the **k**-points weight; E is the energy level of conduction (c) and valence (v) band. The transition dipole moment matrix $\langle \varphi_{c\mathbf{k}} | i\nabla_\alpha - \mathbf{k}_\alpha | \varphi_{v\mathbf{k}} \rangle$ describes the strength of the light–matter interactions in the α polarization direction and the delta function δ ensures energy conservation during interband transitions.

To calculate the dielectric function, we applied the density functional theory (DFT)-based first-principles simulations to solve electrons' Schrodinger equations and obtained the above physical quantities. The Vienna ab initio simulation package (VASP) [36] was chosen to perform the electronic band structure and dielectric function calculations. The exchange and correlation term was described by the generalized gradient approximation (GGA) with the Perdew–Becke–Erzenhof (PBE) functional. Regarding the choice of lattice structure of Ta_2O_5, we chose the monoclinic C2/c structure including 14 atoms in a unit cell [34]. The relaxed lattice parameters were a = 6.917 Å, b = 6.917 Å, c = 5.59 Å, α = 77.65°, β = 77.65°, and γ = 41.74°. That is because, although noncrystalline thin films lack long-range symmetry, the topological constraints hold to some extent and they share some structural properties with the crystalline polymorphs, at least on the local scale. Prior to the dielectric properties calculations, the structural optimization was performed, where the energy cutoff was set as 520 eV and the maximum forces acting on each atom were smaller than 10^{-6} eV/Å. With the relaxed lattice structure, the ground-state electronic energy state and transition dipole moment were calculated to predict the dielectric function [37–40]. With the conventional DFT, the "frozen" atom was adopted and all the properties were predicted at the absolute 0 K. To explore the temperature effect, we applied the first-principles molecular dynamics simulations to introduce lattice vibration effect and to collect the thermally equilibrated configurations at finite temperatures. A large supercell 2 × 2 × 2 containing 112 atoms was built to perform the dynamics simulations. The timestep was set as 1 femosecond (fs) and a 2 picosecond (ps) dynamics run was sufficient to reach thermal equilibrium. In the following 3 ps dynamics run, the thermally equilibrated configurations were collected by

averaging over ten representative configurations. Then, the finite temperature dielectric functions were predicted following the Fermi's golden rule. Moreover, the conventional DFT was based on the independent particle approximation (IPA) and ignore the many-body effect [41]. To study the many-body effect on optical absorption of Ta_2O_5, we performed the model Bethe–Salpeter equation (mBSE) calculations.

3. Results and Discussions

After preparing the Ta_2O_5 thin films following the magnetron sputtering method, we employed an RC2 ellipsometer to measure the complex dielectric function in the ultraviolet-visible spectral range. With the use of a Linkham heat cell, the Ta_2O_5 sample was heated up to 873 K and the ellipsometry parameters (Ψ and Δ) were collected every 100 K. In Figure 1, it is observed that temperature has a nontrivial influence on the ultraviolet-visible dielectric function of Ta_2O_5. The amplitudes of the real part ε_1 and imaginary part ε_2 of the dielectric functions both consistently decrease as the temperature increases from 300 to 873 K. Meanwhile, its absorption edge shifts from 4.052 eV at 300 K to 3.712 eV at 873 K.

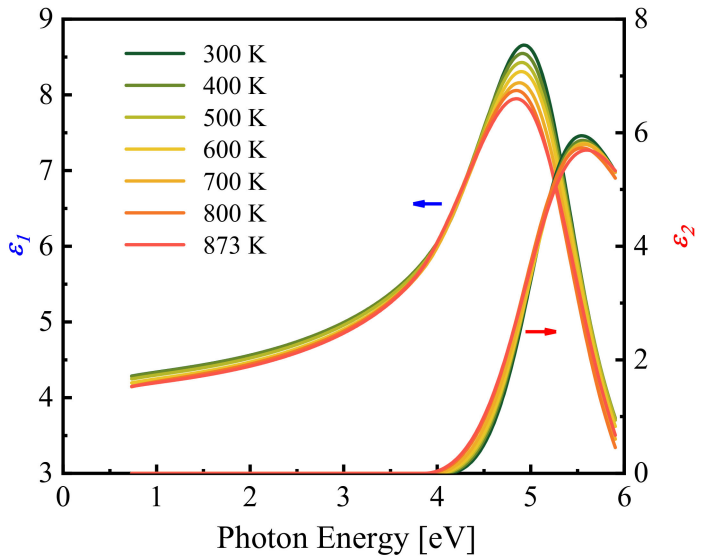

Figure 1. The measured complex dielectric functions of Ta_2O_5 using an RC2 ellipsometer in the ultraviolet-visible spectral range at temperatures varying from 300 to 873 K.

To quantify the temperature influence, we fit the temperature-dependent ε_2 with a Tauc–Lorentz oscillator, expressed by [42]:

$$\varepsilon_2 = \begin{cases} \frac{A_m E_0 B_r (E - E_g)^2}{(E^2 - E_0^2) + B_r{}^2 E^2} \cdot \frac{1}{E} & for\ E > E_g \\ 0 & for\ E \leq E_g \end{cases}, \quad (2)$$

where A_m is the amplitude, E_0 is location of dominant peak, B_r is the broadening width, and E_g is the absorption edge. This oscillator assumes that optical absorption occurs when the incident photon energy is higher than the absorption edge. After data fitting, the temperature-dependent oscillator parameters are obtained. In Figure 2, it shows that A_m linearly reduces as temperature increases, while the parameters E_0 and B_r slightly enlarge. The change trend of A_m and B_r with increasing temperature is normal and easy to understand. The dielectric function reflects the intrinsic strength of light–matter interactions. As temperature increases, the increased lattice vibration significantly influences the electrons' quantum behaviors, leading to reduced relaxation lifetime and perturbed electronic band structure. As a consequence, fewer electrons would participate in the light–matter interactions and the optical absorption strength reduces. However, the locations of dominant absorption E_0 abnormally increase as lattice vibration strengthens. To understand this

phenomenon, we perform first-principles simulations to obtain electronic energy bands, density of states, and their relationships with optical absorption.

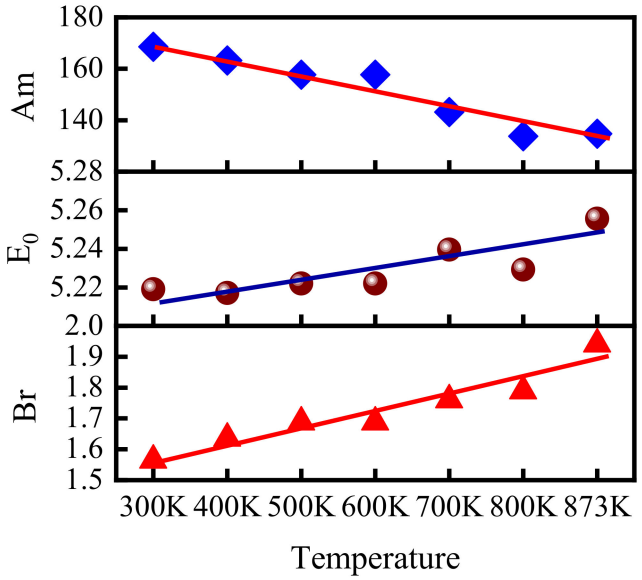

Figure 2. The temperature-dependent parameters of the Tauc–Lorentz oscillator which fits the ultraviolet-visible dielectric functions of Ta_2O_5 thin films measured using an RC2 ellipsometer.

In Figure 3, the electronic band structure, projected density of states, and the square of transition dipole moment of Ta_2O_5 are calculated from first principles. It shows that the valence band maximum (VBM) and conduction band minimum (CBM) locates at different sites in the first Brillouin zone, indicating the indirect band gap of Ta_2O_5. By further analyzing the projected density of states, the top valence bands are mainly contributed by the O_px, O_py, and O_pz orbitals, while the low conduction bands are contributed by the Ta_dx2, Ta_dxz, and Ta_dz2 orbitals. The aggregate of energy states near the VBM and CBM generate a large probability of electronic interband transition. In Figure 3c, there is a dominant peak in the square of transition dipole moment between the VBM and CBM along the high-symmetry G-M line in the first Brillouin zone. The larger the transition dipole moment is, the stronger the optical absorption is. Therefore, this can explain the steep absorption edge in the dielectric function of Ta_2O_5.

After obtaining the fundamental electronic band structure, density of states, and transition dipole moment, the dielectric function can be computed. In Figure 4, we predict the dielectric function of Ta_2O_5 using IPA and mBSE methods. As compared with IPA, the mBSE method considers the many-body effect. The calculation results show that both the IPA and mBSE method can predict the absorption edge of Ta_2O_5, in good agreement with the SE experiments. However, a deviation is observed in the width of the dominant absorption peak. The theoretical calculations over predict the width of the dominant peak. Moreover, the theoretically predicted real part ε_1 by the mBSE method is in better agreement with the SE data than IPA, suggesting the nontrivial influence of many-body effect on optical absorption of Ta_2O_5.

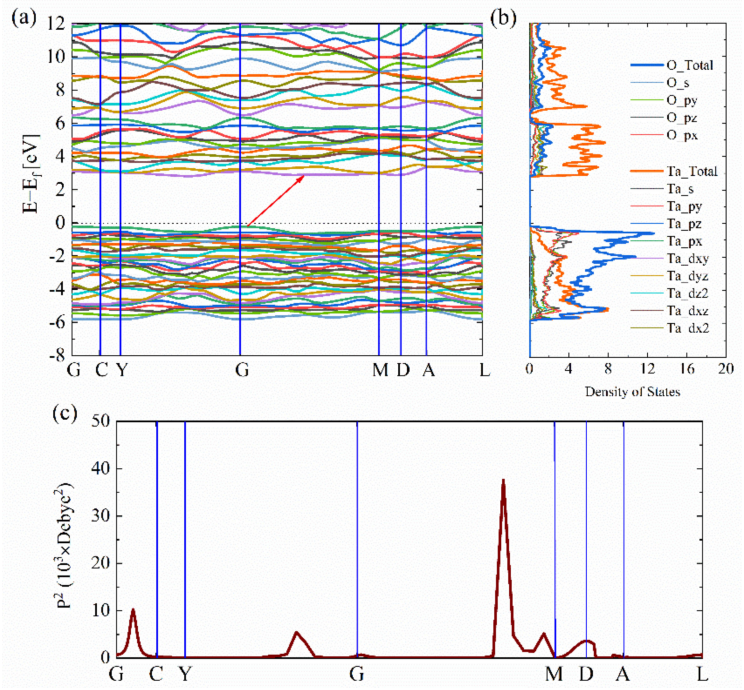

Figure 3. The theoretically calculated: (**a**) electronic band structure; (**b**) projected density of states; (**c**) the square of transition dipole moment, between the valence band maximum (VBM) and the conduction band minimum (CBM).

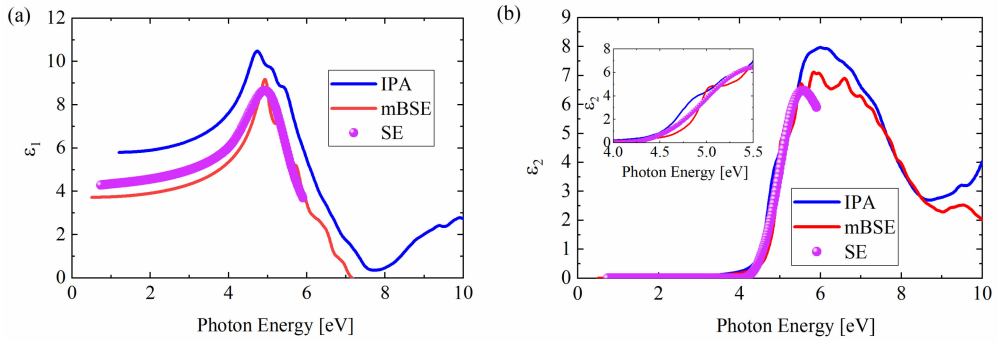

Figure 4. The theoretically predicted: (**a**) real part; (**b**) imaginary part, of the dielectric function of Ta_2O_5 using the independent-particle approximation (IPA) and model Bethe–Salpeter equation (mBSE) approach as compared with SE data at normal conditions. The inset of (**b**) is the enlarged view in the energy spectral range between 3.5 eV and 5.5 eV.

To further understand the temperature effect on electronic band structure and optical properties, we perform first-principles molecular dynamics simulations of Ta_2O_5 at finite temperatures and collect ten thermally equilibrated configurations after the systems reach thermal equilibrium. Then, we perform first-principles calculations to predict the electronic band structure and dielectric function using the IPA method for each configuration, and calculate the average of the dielectric functions of ten configurations at finite temperatures. In Figure 5, the theoretically predicted dielectric functions of Ta_2O_5 at 0 K, 300 K, and 800 K from first principles are presented. The calculation results show that the amplitude of dominant absorption peak decreases as temperature increases, which agrees with the SE experiments. Moreover, the dominant absorption peak slightly shifts to higher energy as the temperature increases, consistent with the SE measurements. However, relatively large optical absorption appears in the low energy range, which deviates from the SE data. After further analyzing the density of states, it is attributed to the greatly modified energy states near the lowest conduction bands. In the thermally equilibrated configurations at finite

temperatures, the crystal symmetry is broken and energy degeneracy is reduced, resulting in the aggregated energy states near the bottom of conduction bands.

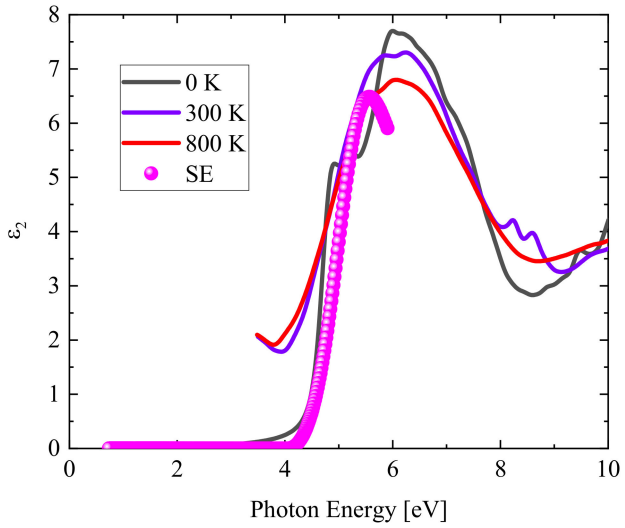

Figure 5. The theoretically predicted dielectric functions of Ta_2O_5 at finite temperatures using first-principles calculations as compared with the SE data.

4. Conclusions

To summarize, we have systematically investigated the ultraviolet-visible dielectric function of Ta_2O_5 and its temperature dependence using combined spectroscopic ellipsometry measurements and first-principles calculations. As temperature increases from 300 to 873 K, the SE experiments observe the linearly decreased amplitude and increased broadening width of the dominant absorption peak locating around 5.2 eV. The first-principles calculation results confirm that the dominant absorption peak arises from the aggregated energy states near the VBM and CBM, and the theoretically predicted dielectric function agrees overall with the SE experiments. To understand the temperature influence, we perform first-principles molecular dynamics simulations to obtain thermally perturbed configurations, and then predict the dielectric function at finite temperatures. The calculation results show that the strengthened lattice vibration break crystal symmetry and reduce energy degeneracy near the lowest conduction bands, which enlarge optical absorption in the low energy spectral range. This work provides the ultraviolet-visible dielectric function of Ta_2O_5 at finite temperatures and an underlying study on its temperature dependence, which could help promote its applications in microelectronic devices.

Author Contributions: Data curation, T.C.; investigation, T.F. and J.Z.; methodology, Z.Z. and Z.F.; resources, X.L.; supervision, J.-Y.Y.; writing—original draft, W.Z. All authors have read and agreed to the published version of the manuscript.

Funding: This research was funded by the National Natural Science Foundation of China (52006127, 52102171) and the Natural Science Foundation of Shandong Province (ZR2020LLZ006 and ZR2020QE194).

Data Availability Statement: The data that support the findings of this study are available from the corresponding author upon reasonable request.

Acknowledgments: J.-Y.Y. is grateful for the support from Shandong University (Qilu Young Scholar 89963031). W.Z. appreciates the support by the fundamental research funds of Shandong University.

Conflicts of Interest: The authors declare no conflict of interest.

References

1. Homes, C.C.; Vogt, T.; Shapiro, S.M.; Wakimoto, S.; Ramirez, A.P. Optical response of high-dielectric-constant perovskite-related oxide. *Science* **2001**, *293*, 673–676. [CrossRef] [PubMed]
2. Krohns, S.; Lunkenheimer, P.; Meissner, S.; Reller, A.; Gleich, B.; Rathgeber, A.; Gaugler, T.; Buhl, H.U.; Sinclair, D.C.; Loidl, A. The route to resource-efficient novel materials. *Nat. Mater.* **2011**, *10*, 899–901. [CrossRef] [PubMed]
3. Zhao, X.-G.; Liu, P.; Song, Y.-C.; Zhang, A.-P.; Chen, X.-M.; Zhou, J.-P. Origin of colossal permittivity in $(In_{1/2}Nb_{1/2})TiO_2$ via broadband dielectric spectroscopy. *Phys. Chem. Chem. Phys.* **2016**, *18*, 26310. [CrossRef] [PubMed]
4. Huang, Y.; Huang, R.; Pan, Y.; Zhang, L.; Cai, Y.; Yang, G.; Wang, Y. A New Dynamic Selector Based on the Bipolar RRAM for the Crossbar Array Application. *IEEE Trans. Electron Devices* **2012**, *59*, 2277–2280. [CrossRef]
5. Xu, H.; Jiang, Y.; Luo, S.; Ma, Y.; Wang, Y. Enhanced dielectric properties of Ti-doped Ta_2O_5 single crystal grown by floating zone technique. *J. Alloys Compd.* **2014**, *588*, 42–45. [CrossRef]
6. Lee, M.J.; Lee, C.B.; Lee, D.; Lee, S.R.; Chang, M.; Hur, J.H.; Kim, Y.-B.; Kim, C.-J.; Seo, D.H.; Seo, S.; et al. A fast, high-endurance and scalable non-volatile memory device made from asymmetric Ta_2O_{5-x}/TaO_{2-x} bilayer structures. *Nat. Mater.* **2011**, *10*, 625–630. [CrossRef] [PubMed]
7. Zhuo, V.Q.; Jiang, Y.; Li, M.H.; Chua, E.K.; Zhang, Z.; Pan, J.S.; Zhao, R.; Shi, L.P.; Chong, T.C.; Robertson, J. Band alignment between Ta_2O_5 and metals for resistive random access memory electrodes engineering. *Appl. Phys. Lett.* **2013**, *102*, 062106. [CrossRef]
8. Roy, P.K.; Kizilyalli, I.C. Stacked high-ε gate dielectric for gigascale integration of metal–oxide–semiconductor technologies. *Appl. Phys. Lett.* **1998**, *72*, 2835–2837. [CrossRef]
9. Markosyan, A.S.; Route, R.; Fejer, M.M.; Patel, D.; Menoni, C. Study of spontaneous and induced absorption in amorphous Ta_2O_5 and SiO_2 dielectric thin films. *J. Appl. Phys.* **2013**, *113*, 133104. [CrossRef]
10. Garavito, J.; Galvis, C.; López, A.; Franco, A.; Barreiro, F.; Tarazona, R.; Serpa-Imbett, C. Heating Device Based on Modified Microwave Oven: Improved to Measure Liquid Temperature by Using FBG Sensors. *Photonics* **2021**, *8*, 104. [CrossRef]
11. Knox, R.S. Principles of the Theory of Solids. *J. Am. Chem. Soc.* **1965**, *87*, 3288. [CrossRef]
12. Ezhilvalavan, S.; Tseng, T.-Y. Preparation and properties of tantalum pentoxide (Ta_2O_5) thin films for ultra large scale integrated circuits (ULSIs) application—A review. *J. Mater. Sci. Mater. Electron.* **1999**, *10*, 9–31. [CrossRef]
13. Shibata, S. Dielectric constants of Ta_2O_5 thin films deposited by r.f. sputtering. *Thin Solid Films* **1996**, *277*, 1–4. [CrossRef]
14. Andreoni, W.; Pignedoli, C.A. Ta_2O_5 polymorphs: Structural motifs and dielectric constant from first principles. *Appl. Phys. Lett.* **2010**, *96*, 062901. [CrossRef]
15. Rathee, K.; Malik, B. Structural and electrical properties of Tantalum Pentaoxide (Ta_2O_5) thin films—A review. *Int. J. Mod. Phys. Conf. Ser.* **2013**, *22*, 564–569. [CrossRef]
16. Bousquet, A.; Zoubian, F.; Cellier, J.; Taviot-Guého, C.; Sauvage, T.; Tomasella, E. Structural and ellipsometric study on tailored optical properties of tantalum oxynitride films deposited by reactive sputtering. *J. Phys. D Appl. Phys.* **2014**, *47*, 475201. [CrossRef]
17. Cheng, T.; Fei, T.; Zhang, W.; Yang, J.-Y.; Liu, L. Ellipsometric and first-principles study on temperature-dependent UV–Vis dielectric functions of GaN. *Appl. Opt.* **2021**, *60*, 6869. [CrossRef]
18. Liu, Y.; Li, Q.X.; Wan, L.Y.; Kucukgok, B.; Ghafari, E.; Ferguson, I.T.; Zhang, X.; Wang, S.; Feng, Z.C.; Lu, N. Composition and temperature dependent optical properties of $Al_xGa_{1-x}N$ alloy by spectroscopic ellipsometry. *Appl. Surf. Sci.* **2017**, *421*, 389–396. [CrossRef]
19. Shokhovets, S.; Goldhahn, R.; Gobsch, G.; Piekh, S.; Lantier, R.; Rizzi, A.; Lebedev, V.; Richter, W. Determination of the anisotropic dielectric function for wurtzite AlN and GaN by spectroscopic ellipsometry. *J. Appl. Phys.* **2003**, *94*, 307–312. [CrossRef]
20. Li, Q.H.; Zhu, D.; Liu, W.; Liu, Y.; Ma, X.C. Optical properties of Al-doped ZnO thin films by ellipsometry. *Appl. Surf. Sci.* **2008**, *254*, 2922–2926. [CrossRef]
21. Zhang, X.; Qiu, J.; Li, X.; Zhao, J.; Liu, L.H. Complex refractive indices measurements of polymers in visible and near-infrared bands. *Appl. Opt.* **2020**, *59*, 2337–2344. [CrossRef]
22. Karmakov, I.; Konova, A.; Atanassova, E.; Paskaleva, A. Spectroscopic ellipsometry of very thin tantalum pentoxide on Si. *Appl. Surf. Sci.* **2009**, *255*, 9211–9216. [CrossRef]
23. Zhang, D.X.; Zheng, Y.X.; Cai, Q.Y.; Lin, W.; Wu, K.N.; Mao, P.H.; Zhang, R.-J.; Zhao, H.-B.; Chen, L.-Y. Thickness-dependence of optical constants for Ta_2O_5 ultrathin films. *Appl. Phys. A* **2012**, *108*, 975–979. [CrossRef]
24. Franke, E.; Trimble, C.L.; Devries, M.J.; Woollam, J.A.; Schubert, M.; Frost, F. Dielectric function of amorphous tantalum oxide from the far infrared to the deep ultraviolet spectral region measured by spectroscopic ellipsometry. *J. Appl. Phys.* **2000**, *88*, 5166–5174. [CrossRef]
25. Franke, E.; Schubert, M.; Trimble, C.; DeVries, M.; Woollam, J. Optical properties of amorphous and polycrystalline tantalum oxide thin films measured by spectroscopic ellipsometry from 0.03 to 8.5 eV. *Thin Solid Films* **2011**, *388*, 283–289. [CrossRef]
26. Prachachet, R.; Buranasiri, P.; Horprathum, M.; Eiamchai, P.; Limwichean, S.; Patthanasettakul, V.; Nuntawong, N.; Chindaudom, P.; Samransuksamer, B.; Lertvanithphol, T. Investigation of optical characteristics of the evaporated Ta_2O_5 thin films based on ellipsometry and spectroscopy. *Mater. Today Proc.* **2017**, *4*, 6365–6371. [CrossRef]
27. Darmasetiawan, H.; Irzaman, I.; Indro, M.N.; Sukaryo, S.; Hikam, M.; Bo, N.P. Optical Properties of Crystalline Ta_2O_5 Thin Films. *Phys. Status Solidi A* **2002**, *193*, 53–60. [CrossRef]

28. Yang, J.-Y.; Cheng, T.; Fei, T.; Zhang, C.; Liu, L. Temperature-induced surface phonon polaritons dissipation in perovskite $SrTiO_3$. *Opt. Lett.* **2021**, *46*, 4244–4247. [CrossRef]
29. Ivanov, M.V.; Perevalov, T.V.; Aliev, V.S.; Gritsenko, V.A.; Kaichev, V.V. Electronic structure of δ-Ta_2O_5 with oxygen vacancy: Ab initio calculations and comparison with experiment. *J. Appl. Phys.* **2011**, *110*, 024115. [CrossRef]
30. Lee, J.; Lu, W.D.; Kioupakis, E. Electronic and optical properties of oxygen vacancies in amorphous Ta_2O_5 from first principles. *Nanoscale* **2017**, *9*, 1120–1127. [CrossRef] [PubMed]
31. Kim, J.-Y.; Magyari-Köpe, B.; Nishi, Y.; Ahn, J.-H. First-principles study of carbon impurity effects in the pseudo-hexagonal Ta_2O_5. *Curr. Appl. Phys.* **2016**, *16*, 638–643. [CrossRef]
32. Valencia-Balvín, C.; Pérez-Walton, S.; Osorio-Guillén, J.M. First principles calculations of the electronic and dielectric properties of λ-Ta_2O_5. *TecnoLogicas* **2018**, *21*, 43–52. [CrossRef]
33. Chu, A.K.; Lin, H.C.; Cheng, W.H. Temperature dependence of refractive index of Ta_2O_5. *J. Electron. Mater.* **1997**, *26*, 889–892. [CrossRef]
34. Liu, X.; Han, X.; Zhang, Z.; Ji, L.; Jiang, Y. The crystal structure of high temperature phase Ta_2O_5. *Acta Mater.* **2007**, *55*, 2385–2396. [CrossRef]
35. Gajdoš, M.; Hummer, K.; Kresse, G.; Furthmüller, J.; Bechstedt, F. Linear optical properties in the projector-augmented wave methodology. *Phys. Rev. B* **2006**, *73*, 045112. [CrossRef]
36. Kresse, G.; Furthmüller, J. Efficient iterative schemes for ab initio total-energy calculations using a plane-wave basis set. *Phys. Rev. B* **1996**, *54*, 11169–11186. [CrossRef]
37. Yang, J.; Liu, L.; Tan, J. First-principles molecular dynamics study on temperature-dependent dielectric function of bulk 3C and 6H SiC in the energy range 3–8 eV. *Phys. B Condens. Matt.* **2014**, *436*, 182–187. [CrossRef]
38. Marini, A. Ab initio finite-temperature excitons. *Phys. Rev. Lett.* **2008**, *101*, 106405. [CrossRef]
39. Ghandchi, M.; Darvish, G.; Moravvej-Farshi, M.K. Properties of Bilayer Graphene Quantum Dots for Integrated Optics: An Ab Initio Study. *Photonics* **2020**, *7*, 78. [CrossRef]
40. Yang, J.; Liu, L.; Tan, J. Temperature-dependent dielectric function of germanium in the UV–vis spectral range: A first-principles study. *J. Quant. Spectrosc. Radiat. Transf.* **2014**, *141*, 24–30. [CrossRef]
41. Rohlfing, M.; Louie, S.G. Excitonic effects and the optical absorption spectrum of hydrogenated Si clusters. *Phys. Rev. Lett.* **1998**, *80*, 3320. [CrossRef]
42. Von Blanckenhagen, B.; Tonova, D.; Ullmann, J. Application of the Tauc-Lorentz formulation to the interband absorption of optical coating materials. *Appl. Opt.* **2002**, *41*, 3137–3141. [CrossRef] [PubMed]